5-10-2000

The Peculiar Type Ic Supernova 1997ef: Another Hypernova

Koichi Iwamoto
Nihon University

Takayoshi Nakamura
University of Tokyo

Ken'ichi Nomoto
University of Tokyo

Paolo A. Mazzali
Osservatorio Astronomico di Trieste

I. John Danziger
Osservatorio Astronomico di Trieste

See next page for additional authors

THE ASTROPHYSICAL JOURNAL, 534:660–669, 2000 May 10

THE PECULIAR TYPE Ic SUPERNOVA 1997ef: ANOTHER HYPERNOVA

KOICHI IWAMOTO,[1] TAKAYOSHI NAKAMURA,[2] KEN'ICHI NOMOTO,[2,3] PAOLO A. MAZZALI,[3,4] I. JOHN DANZIGER,[4]
PETER GARNAVICH,[5] ROBERT KIRSHNER,[5] SAURABH JHA,[5] DAVID BALAM,[6] AND JOHN THORSTENSEN[7]
Received 1998 May 26; accepted 2000 January 4

ABSTRACT

SN 1997ef has been recognized as a peculiar supernova from its light curve and spectral properties. The object was classified as a Type Ic supernova (SN Ic) because its spectra were dominated by broad absorption lines of oxygen and iron, lacking any clear signs of hydrogen or helium line features. The light curve is very different from that of previously known SNe Ic, showing a very broad peak and a slow tail. The strikingly broad line features in the spectra of SN 1997ef, which were also seen in the hypernova SN 1998bw, suggest the interesting possibility that SN 1997ef may also be a hypernova. The light curve and spectra of SN 1997ef were modeled first with a standard SN Ic model assuming an ordinary kinetic energy of explosion $E_K = 10^{51}$ ergs. The explosion of a CO star of mass $M_{\rm CO} \approx 6\ M_\odot$ gives a reasonably good fit to the light curve but clearly fails to reproduce the broad spectral features. Then, models with larger masses and energies were explored. Both the light curve and the spectra of SN 1997ef are much better reproduced by a C+O star model with $E_K = 8 \times 10^{51}$ ergs and $M_{\rm CO} = 10\ M_\odot$. Therefore, we conclude that SN 1997ef is very likely a hypernova on the basis of its kinetic energy of explosion. Finally, implications for the deviation from spherical symmetry are discussed in an effort to improve the fits to the observations.

Subject headings: galaxies: individual (UGC 4107) — radiative transfer — supernovae: individual (SN 1997ef)

1. INTRODUCTION

The supernova 1997ef (SN 1997ef) was discovered on 1997 November 25 at an *R* magnitude of 16.7 near the spiral galaxy UGC 4107 (Sano 1997). The first spectrum was taken on November 26 (Garnavich et al. 1997a). Subsequently, photometric and spectroscopic follow-ups have provided high-quality optical light curves and spectra (Garnavich et al. 1997a, 1997b, 1997c; Hu et al. 1997; Filippenko 1997; Wang & Wheeler 1998). As seen in Figure 1, the spectra of SN 1997ef are dominated by broad oxygen and iron lines but do not show any clear feature of hydrogen or helium (Garnavich et al. 1997c; Filippenko et al. 1997), showing the overall similarity to other Type Ic supernovae (SNe Ic) SN 1994I and SN 1998bw. This led us to classify SN 1997ef as a SN Ic.

In Figure 2 the visual light curve of SN 1997ef (Garnavich et al. 1997b, 1997c) is compared with those of the SN Ic SN 1998bw (Galama et al. 1998) and the ordinary SN Ic SN 1994I (Richmond et al. 1996a, 1996b). Despite the spectral similarity, the light curve of SN 1997ef is quite different from those of SN 1998bw and SN 1994I. It has quite a flat peak, much broader than those of the other SNe Ic. Besides, the tail of the light curve of SN 1997ef starts late and the rate of its decline is much slower than in other SNe Ic. It is also true that the light curves are rather diverse, even in this limited number of samples, implying a range of energies and/or progenitor masses of SN Ic explosions.

The most striking and peculiar characteristic of SN 1997ef is the breadth of its line features. Such broad spectral features were later recognized to be a distinguishing property of the spectra in SN 1998bw (Fig. 1). SN 1998bw was discovered within the error box of GRB 980425 determined by the *BeppoSAX* satellite, only 0.9 days after the date of the gamma-ray burst (GRB), and therefore probably related to this GRB (Galama et al. 1998). The very broad spectral features and the light-curve shape have led to the conclusion that SN 1998bw had an extremely large *kinetic* energy of explosion, $E_K \sim 3 \times 10^{52}$ ergs (Iwamoto et al. 1998; Woosley, Eastman, & Schmidt 1999). This was 1 order of magnitude larger than the energy of typical supernovae; thus, SN 1998bw was termed a "hypernova" (Iwamoto et al. 1998).

The spectral similarities between SN 1997ef and SN 1998bw suggest the interesting possibility that SN 1997ef may also be a hypernova. In fact, a possible connection with a GRB has been suggested for SN 1997ef: GRB 971115 appears to be compatible with the supernova in the position and the time of occurrence (Wang & Wheeler 1998). Since the statistical significance for this case is much weaker than for the case of SN 1998bw and GRB 980425, it is difficult to confirm the physical association between SN 1997ef and GRB 971115. However, it is possible at least to clarify whether or not SN 1997ef is a hypernova by estimating the kinetic energy of explosion through modeling of light curves and spectra as in the case of SN 1998bw (Iwamoto et al. 1998; Mazzali 1999). This is exactly the primary purpose of this paper.

We constructed supernova progenitor models and performed detailed hydrodynamics and radiation transfer cal-

[1] Department of Physics, College of Science and Technology, Nihon University, Chiyoda-ku, Tokyo 101-8308, Japan.
[2] Department of Astronomy, School of Science, University of Tokyo, Bunkyo-ku, Tokyo 113-0033, Japan.
[3] Research Center for the Early Universe, School of Science, University of Tokyo, Bunkyo-ku, Tokyo 113-0033, Japan.
[4] Osservatorio Astronomico di Trieste, via G. B. Tiepolo 11, I-34131 Trieste, Italy.
[5] Harvard-Smithsonian Center for Astrophysics, 60 Garden Street, Cambridge, MA 02138.
[6] University of Victoria, Victoria, BC, Canada.
[7] Dartmouth College, Department of Physics and Astronomy, Hanover, NH 03755.

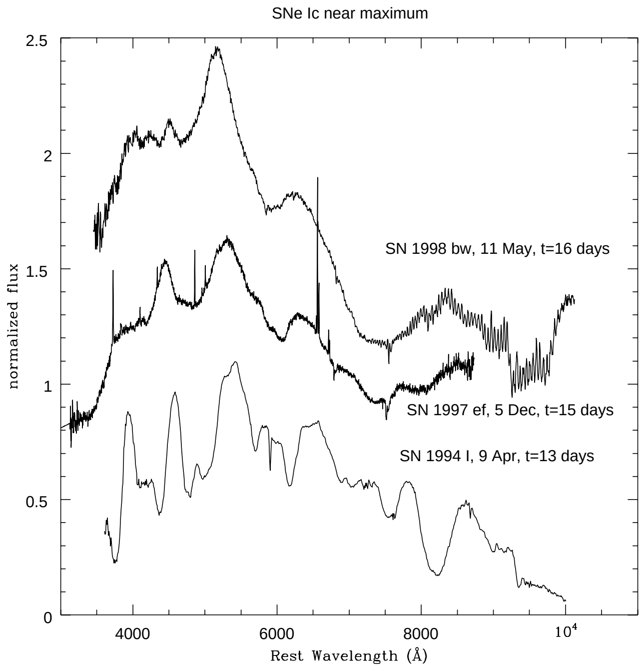

FIG. 1.—Observed spectra of Type Ic supernovae SN 1997ef, SN 1998bw, and SN 1994I.

culations to obtain light curves and spectra for the explosion models. The results were compared with observations of SN 1997ef in order to derive its explosion energy and the ejecta mass and thus to determine whether SN 1997ef was an ordinary SN Ic or a hypernova. Since the light curves of the other SNe Ic SN 1994I and SN 1998bw were successfully reproduced by the collapse-induced explosion of C+O stars (Nomoto et al. 1994; Iwamoto et al. 1994, 1998), we adopted C+O stars as progenitor models for SN 1997ef as well.

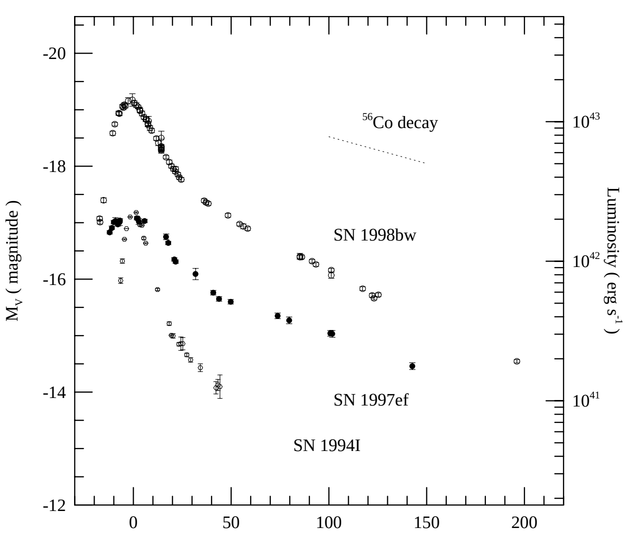

FIG. 2.—Absolute magnitudes of Type Ic supernovae: the ordinary SN Ic SN 1994I (Richmond et al. 1996a, 1996b), the hypernova SN 1998bw (Galama et al. 1998), and the proposed hypernova SN 1997ef. The dashed line indicates the ^{56}Co decay rate.

This paper consists of six sections including this introduction. Section 2 describes the ordinary SN Ic model and the hypernova model. The method and results of our light-curve calculations are presented in § 3. The synthetic spectra are compared with the observations in § 4. Section 5 is devoted to discussion on various issues including the SN-GRB connection and possible progenitor scenarios. Finally, our conclusions are summarized in § 6.

2. EXPLOSION MODELS FOR SUPERNOVAE AND HYPERNOVAE

We construct hydrodynamical models of an ordinary SN Ic and a hypernova as follows.

1. In the ordinary SN Ic model (model CO60), a C+O star with a mass $M_{CO} = 6.0\ M_\odot$ (which is the core of a 25 $M_\odot$ main-sequence star) explodes with kinetic energy of explosion $E_K = 1.0 \times 10^{51}$ ergs and ejecta mass $M_{ej} = M_{CO} - M_{rem} = 4.6\ M_\odot$. Here M_{rem} ($=1.4\ M_\odot$) denotes the mass of the compact star remnant (either a neutron star or a black hole).
2. In the hypernova model (CO100), a C+O star of $M_{CO} = 10.0\ M_\odot$ is constructed from the 10 $M_\odot$ He star (which has an 8 $M_\odot$ C+O core) by removing the outermost 2 $M_\odot$ of He layer and extending the C+O layer up to 10.0 $M_\odot$. This model corresponds to 30–35 $M_\odot$ on the main sequence. This progenitor goes off with $E_K = 8.0 \times 10^{51}$ ergs and $M_{ej} = 7.6\ M_\odot$, i.e., $M_{rem} = 2.4\ M_\odot$.

The hydrodynamics at early phases was calculated by using a Lagrangian PPM code (Colella & Woodward 1984) with a simple nuclear reaction network including 13 alpha elements (Müller 1986). Detailed postprocessing calculations were carried out with a larger size nuclear reaction network including 240 isotopes (Hix & Thielemann 1996). The explosion is triggered by depositing thermal energy in a couple of zones just below the mass cut so that the final kinetic energy becomes the required value. The position of the mass cut is adjusted for the ejected mass of ^{56}Ni to be $M(^{56}\mathrm{Ni}) = 0.15\ M_\odot$.

The compact remnant in CO60 is likely a neutron star because $M_{rem} = 1.4\ M_\odot$, while it may be a black hole in CO100 because M_{rem} ($=2.4\ M_\odot$) may well exceed the maximum mass of a stable neutron star. The above values of M_{rem} are determined so that $M(^{56}\mathrm{Ni}) = 0.15\ M_\odot$ is ejected to reproduce the maximum brightness of SN 1997ef by the radioactive decay heating of ^{56}Ni and ^{56}Co.

These model parameters are summarized in Table 1. They can be constrained by comparing the calculated light curves and synthetic spectra with observations. The parameters of models CO21 for SN 1994I (Nomoto et al. 1994; Iwamoto et al. 1994) and CO138 for SN 1998bw (Iwamoto et al. 1998) are also given in Table 1. We constructed the progenitor model by attaching a thin hydrostatic and in-thermal-equilibrium C+O envelope to the C+O core of the presupernova model (Nomoto & Hashimoto 1988; Hashimoto 1995).

The expansion soon becomes homologous so that $v \propto r$. The solid lines in Figure 3 show the density distributions in the velocity space for CO60 and CO100 at $t = 16$ days. The expansion velocities are clearly higher in CO100 than in CO60. Figures 4 and 5 show the composition structure of

TABLE 1

PARAMETERS OF THE CO STAR MODELS

Model	C+O Core Mass ($M_\odot$)	Ejecta Mass ($M_\odot$)	^{56}Ni Mass ($M_\odot$)	E_K (10^{51} ergs)
CO21	2.1	0.9	0.07	1
CO60	6.0	4.4	0.15	1
CO100	10.0	7.6	0.15	8
CO138	13.8	10.8	0.7	~30

models CO60 and CO100, respectively, against the expansion velocity and the Lagrangian mass coordinate of the progenitor. In CO100, the Fe and Si-rich layers expand much faster than in CO60. The total amount of nucleosynthesis products are summarized in Table 2.

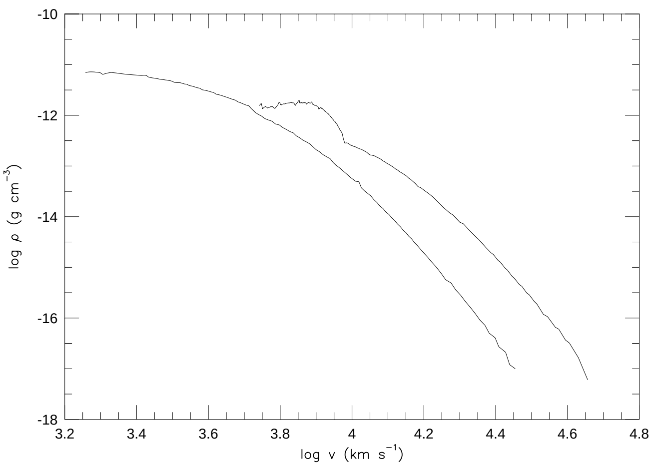

FIG. 3.—Density distributions against the velocity of homologously expanding ejecta for CO60 and CO100

3. LIGHT-CURVE MODELS

3.1. *Radiation Hydrodynamics Code*

The light-curve calculation is started, when the ejecta have reached the homologous expansion phase, with a one-dimensional spherically symmetric radiation transfer code (Iwamoto 1997).

The code solves the multifrequency radiative transfer equation for the specific intensity I_ν in the comoving frame, including all terms up to the first order in v/c (Mihalas & Mihalas 1984):

$$\frac{1}{c}\frac{\partial I_\nu}{\partial t} + \frac{\mu}{r^2}\frac{\partial}{\partial r}(r^2 I_\nu) + \frac{\partial}{\partial \mu}\left\{(1-\mu^2)\left[\frac{1}{r} + \frac{\mu}{c}\left(\frac{v}{r} - \frac{\partial v}{\partial r}\right)\right]I_\nu\right\}$$
$$- \frac{\partial}{\partial \nu}\left\{\nu\left[(1-\mu^2)\frac{v}{cr} + \frac{\mu^2}{c}\frac{\partial v}{\partial r}\right]I_\nu\right\}$$
$$+ \left[(3-\mu^2)\frac{v}{cr} + \frac{1+\mu^2}{c}\frac{\partial v}{\partial r}\right]I_\nu$$
$$= \kappa_\nu B_\nu - \kappa_\nu I_\nu - \sigma_\nu I_\nu + \frac{1}{4\pi}\int \sigma_\nu I_\nu \, d\Omega\,, \quad (1)$$

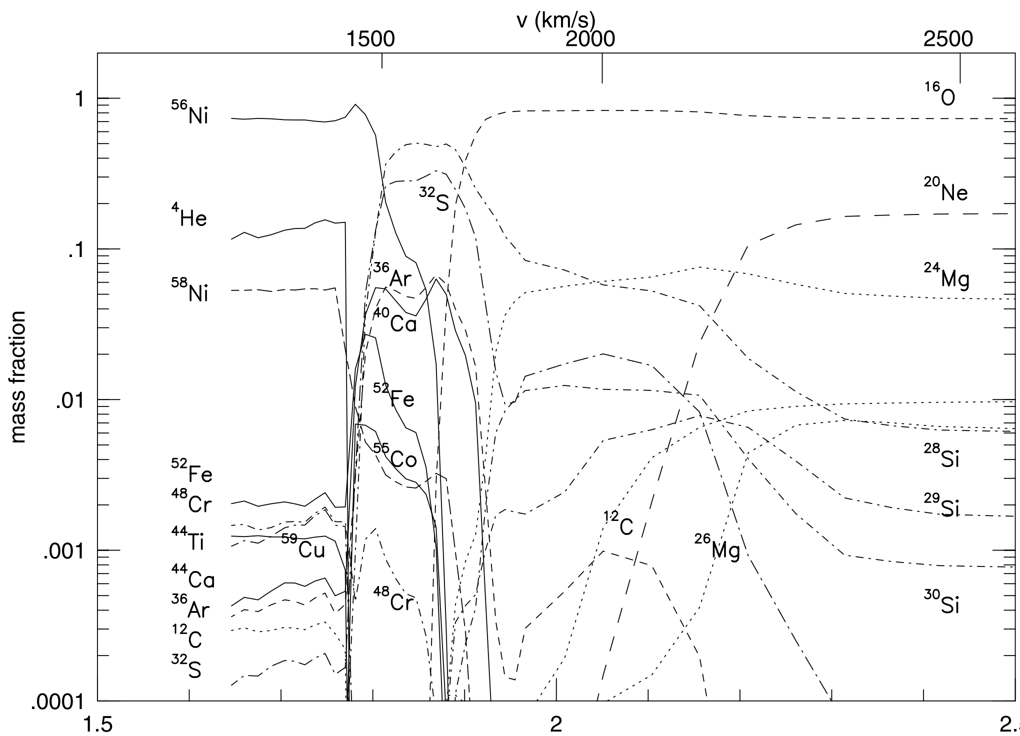

FIG. 4.—Chemical composition of model CO60 plotted against the expansion velocity

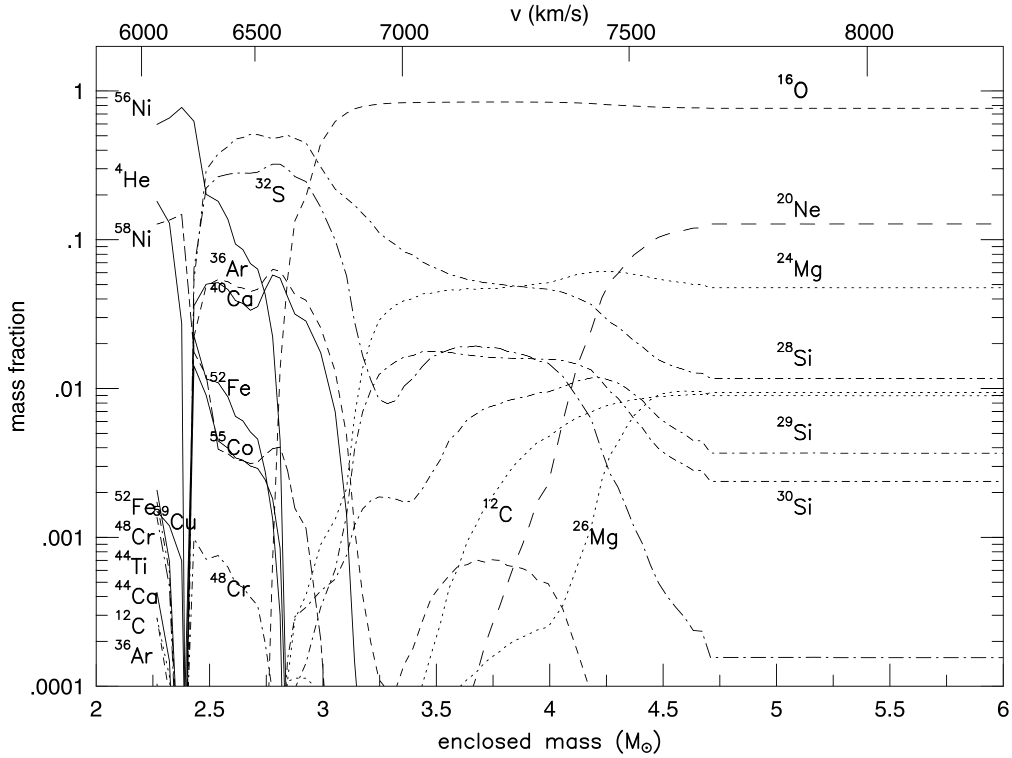

FIG. 5.—Chemical composition of model CO100 plotted against the expansion velocity. Note that this is the result of the nucleosynthesis calculation with a spherically symmetric model and that the light curve computation, ^{56}N, is distributed homogeneously as explained in the text.

where κ_ν and σ_ν are the absorptive and scattering opacities, respectively, B_ν is the Planck function, and μ is the cosine of the angle made by the radial direction and the direction of the ray. This equation is solved numerically using the Feautrier method with an approximate lambda operator similar to the one described by Hauschildt (1992).

To determine the gas temperatures, equation (1) is solved simultaneously with the energy equation and the first two moment equations of equation (1). The energy equation of the radiation plus gas is written as

$$\frac{\partial}{\partial t}\left(e + \frac{E}{\rho}\right) = \epsilon - (P + fE)\,\frac{\partial}{\partial t}\left(\frac{1}{\rho}\right) - 4\pi\,\frac{\partial}{\partial M_r}\,(r^2 F) + (3f - 1)\,\frac{vE}{\rho r}\,, \qquad (2)$$

while the radiation energy and momentum equations are

$$\frac{\partial}{\partial t}\left(\frac{E}{\rho}\right) = \frac{c}{\rho}\,(\kappa_P\, a T^4 - \kappa_E\, E) - fE\,\frac{\partial}{\partial t}\left(\frac{1}{\rho}\right) - 4\pi\,\frac{\partial}{\partial M_r}\,(r^2 F) + (3f - 1)\,\frac{vE}{\rho r}\,, \qquad (3)$$

and

$$\frac{\partial F}{\partial t} = -\left(c\chi_F + \frac{2v}{r}\right)F - 4\pi r^2 \rho \times \left(c^2\,\frac{\partial(fE)}{\partial M_r} + 2F\,\frac{\partial v}{\partial M_r}\right) - (3f - 1)\,\frac{c^2 E}{r}\,, \qquad (4)$$

respectively, where e is the thermal energy of ions and electrons per unit mass, and E, F, and f are the radiation energy density, flux, and the Eddington factor defined as follows:

$$E = \frac{2\pi}{c}\int_0^\infty d\nu \int_{-1}^{1} I_\nu\, d\mu\,, \qquad (5)$$

$$F = 2\pi \int_0^\infty d\nu \int_{-1}^{1} I_\nu\, \mu\, d\mu\,, \qquad (6)$$

$$f = \frac{\int_0^\infty d\nu \int_{-1}^{1} I_\nu \mu^2\, d\mu}{\int_0^\infty d\nu \int_{-1}^{1} I_\nu\, d\mu}\,. \qquad (7)$$

Partial derivatives with respect to t in equations (1)–(4) are all Lagrangian time derivatives. The absorptive and scattering parts of the opacity are given as

$$\kappa_\nu = \epsilon(\kappa_{\text{b-b}} + \kappa_{\text{b-f}}) + \kappa_{\text{f-f}}\,, \qquad (8)$$

and

$$\sigma_\nu = (1 - \epsilon)(\kappa_{\text{b-b}} + \kappa_{\text{b-f}}) + n_e\,\sigma_{\text{T}}\,, \qquad (9)$$

TABLE 2

PREDICTED YIELDS OF SN1997EF ($M_\odot$)

Model	C	O	Si	S	Ca	Fe	^{44}Ti	^{56}Ni	^{57}Ni
CO60	5.2×10^{-2}	3.0	0.10	3.7×10^{-2}	5.7×10^{-3}	0.16	2.1×10^{-4}	0.15	5.7×10^{-3}
CO100	0.58	5.6	0.42	0.19	2.5×10^{-2}	0.19	4.5×10^{-5}	0.15	5.7×10^{-3}

$\kappa_{\text{b-b}}$, $\kappa_{\text{b-f}}$, and $\kappa_{\text{f-f}}$ are the bound-bound, bound-free, and free-free opacities, respectively; n_e is the number density of free electrons, and σ_{T} is the Thomson scattering cross section. In the moment equations, the energy mean (κ_E) and the Planck mean opacities (κ_{P}) include only the absorptive part, while the flux mean opacity (χ_F) is the total opacity.

For bound-bound transitions, energy levels and transition probabilities are taken from the compilation by Kurucz (1991). For bound-free data, we use the analytic fitting formula to the photoionization cross sections given by Verner & Yakovlev (1995). Local thermodynamic equilibrium (LTE) is assumed to determine the ionization balance and the level populations of each ion. However, the non-LTE effect is approximately taken into account by assuming that the value of the absorptive fraction ϵ is a constant less than unity in equations (8) and (9). Experiments of spectral syntheses have shown that a value $\epsilon = 0.1$ is a reasonable choice for this fraction (Baron et al. 1996).

We neglected the effect of relative motion within the ejecta, i.e., the expansion effect, in evaluating the mean opacities, although this is one of the currently controversial issues. It has been argued by several authors that the expansion would increase the chance of interactions between radiation and matter through line transitions, and thus the mean opacities become larger than in static medium, especially at relatively early phases (Karp, Lasher, & Chan 1977; Eastman & Pinto 1993; Blinnikov 1996).

The energy deposition due to the radioactive decays is calculated with a one energy-group γ-ray–transfer code (Iwamoto 1997). We assume an absorptive opacity $\kappa_\gamma = 0.03$ and the complete trapping of positrons. The rest-frame flux is calculated from the comoving-frame intensities using the following transformation:

$$F_{\nu,\text{rest}} = 2\pi \int_{-1}^{1} (\mu + \beta) I\left(\mu, \frac{\nu}{1 + \beta\mu}\right) d\mu \,, \tag{10}$$

$$F_{\lambda,\text{rest}} = \frac{\nu^2}{c} F_{\nu,\text{rest}} \,. \tag{11}$$

For the calculation of the light curves of CO60 and CO100 discussed in the next subsection, we use about 200 radial mesh points to solve the moment equations (2)–(4), while 800 frequency and 50 radial mesh points were used for the multifrequency radiative transfer equation (1).

3.2. *Light-Curve Models*

In Figure 6 we compare the calculated V light curves for models CO60 and CO100 with the observed V light curve of SN 1997ef. We adopt a distance of 52.3 Mpc (a distance modulus of $\mu = 33.6$ mag) as estimated from the recession velocity, 3,400 km s^{-1} (Garnavich et al. 1997a) and a Hubble constant $H_0 = 65$ km s^{-1} Mpc^{-1}. We assume no color excess [$E(B-V) = 0.00$]; this is justified by the fact that no signature of a narrow Na I D interstellar absorption line is visible in the spectra of SN 1997ef at any epochs (Garnavich et al. 1997a). The light curve of SN 1997ef has a very broad maximum, which lasts for $\sim$25 days. This is much broader than in both the ordinary SN Ic 1994I and the hypernova SN 1998bw. The light-curve tail of SN 1997ef starts only $\sim$40 days after maximum, much later than in other SNe Ic.

The light curve of SN 1997ef can be reproduced basically with various explosion models with different energies and masses. In general, the properties of the light curve are characterized by the decline rate in the tail and the peak width, τ_{peak}. The peak width scales approximately as

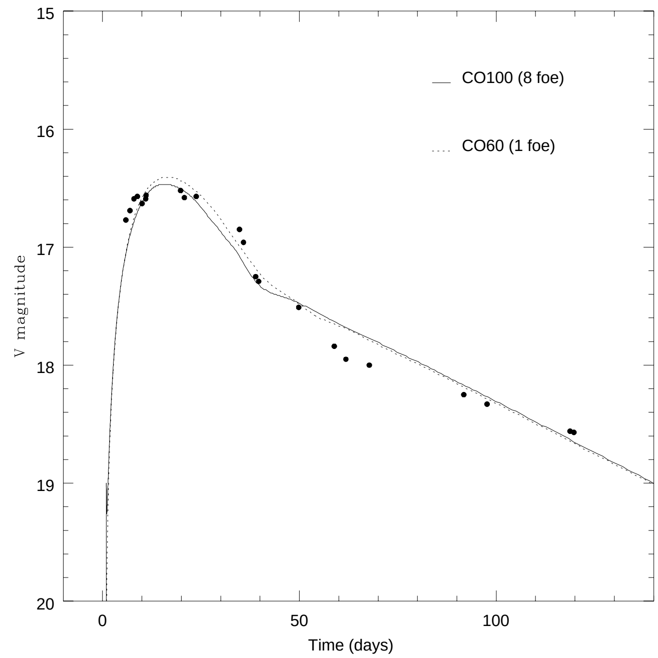

FIG. 6.—Calculated visual light curves of CO60 and CO100 compared with that of SN 1997ef.

$$\tau_{\text{peak}} \propto \kappa^{1/2} M_{\text{ej}}^{3/4} E_K^{-1/4} \,, \tag{12}$$

where κ denotes the optical opacity (Arnett 1996). This is the timescale on which photon diffusion and hydrodynamical expansion become comparable. Since the model parameters of CO100 and CO60 give similar τ_{peak}, the light curves of the two models look similar: both have quite a broad peak and reproduce the light curve of SN1997ef reasonably well (Fig. 6).

The light-curve shape depends also on the distribution of ^{56}Ni, which is produced in the deepest layers of the ejecta. More extensive mixing of ^{56}Ni leads to an earlier rise of the light curve. For SN 1997ef, the best fit is obtained when the ^{56}Ni is mixed almost uniformly to the surface for both models. Without such extensive mixing, the rise time to $V = 16.5$ mag would be $\sim$30 days for CO100, which is clearly too long to be compatible with the spectroscopic dating (see § 4).

Model CO60 has the same kinetic energy ($E_K = 1 \times 10^{51}$ ergs) as model CO21, which was used for SN Ic 1994I (see Table 1 for the model parameters). Since the light curve of SN 1997ef is much slower than that of SN 1994I, the ejecta mass of CO60 is $\sim$5 times larger than that of CO21.

The ejecta mass of CO100 is a factor of $\sim$2 larger than that of CO60, and it is only $\sim$20% smaller than that of model CO138, which was used for SN 1998bw (Table 1). Thus the explosion energy of CO100 should be $\sim$8 times larger than that of CO60 to reproduce the light curve of SN 1997ef. This explosion is very energetic but still much weaker than the one in CO138. The smaller E_K for a comparable mass allows CO100 to reproduce the light curve of SN 1997ef, which has a much broader peak than that of SN 1998bw.

The light curve of SN 1997ef enters the tail around day 40. Since then, the observed V magnitude declines linearly

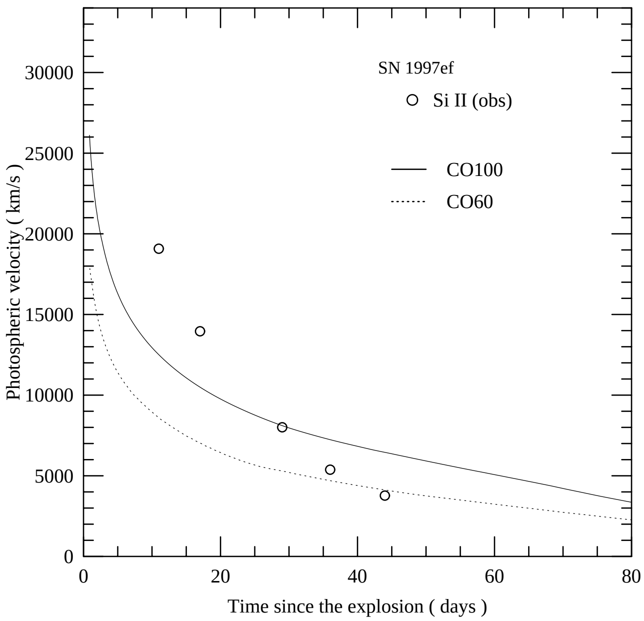

FIG. 7.—Evolution of the calculated photospheric velocities of CO60 and CO100 (*solid lines*) compared with the observed velocities of the Si II 634.7, 637.1 nm line measured in the spectra at the absorption core.

with time at a rate of $\sim 1.1 \times 10^{-2}$ mag day^{-1}, which is slower than in other SNe Ic and is even close to the ^{56}Co decay rate 9.6×10^{-3} mag day^{-1}. Such a slow decline implies much more efficient γ-ray trapping in the ejecta of SN 1997ef than in SN 1994I. The ejecta of both CO100 and CO60 are fairly massive and are able to trap a large fraction of the γ-rays, so that the calculated light curves have slower tails compared with CO21.

However, the light curves for both models decline somewhat faster in the tail than the observations. A similar discrepancy has been noted for the Type Ib supernovae (SNe Ib) SN 1984L and SN 1985F (Swartz & Wheeler 1991; Baron, Young, & Branch 1993). The late-time light-curve decline of these SNe Ib is as slow as the ^{56}Co decay rate, so that the inferred value of M is significantly larger (and/or E_K is smaller) than those obtained by fitting the early light-curve shape. Baron et al. (1993) suggested that the ejecta of these SNe Ib must be highly energetic and as massive as $\sim 50\ M_\odot$. In § 5.1, we will suggest that such a discrepancy between the early- and late-time light curves might be an indication of asphericity in the ejecta of SN 1997ef and that it might be the case in those SNe Ib as well.

3.3. *Photospheric Velocities*

As we have shown, light-curve modeling provides direct constraints on $M_{\rm CO}$ and E_K. However, it is difficult to distinguish between the ordinary SN Ic and the hypernova model from the light-curve shape alone, since models with different values of $M_{\rm ej}$ and E_K can reproduce similar light curves. However, these models are expected to show different evolutions of the photospheric velocity and the spectrum as will be discussed in the following sections.

The photospheric velocity scales roughly as $v_{\rm ph} \propto M_{\rm ej}^{-1/2} E_K^{1/2}$, so that $M_{\rm ej}$ and E_K can be constrained by $v_{\rm ph}$ in a different way from by means of the light-curve width. Figure 7 shows the evolution of the observed velocities of the Si II line measured in the spectra at the absorption core, and the velocities at the gray photosphere computed by the light-curve code for models CO60 and CO100. The velocities of the Si II line are somewhat higher than that of the photosphere, reaching $\sim 20{,}000$ km s^{-1} at the earliest time.

In model CO60 the photosphere forms at velocities much smaller than those of the observed lines, while CO100 gives photospheric velocities as high as the observed ones. It is clear, from this comparison, that the hyperenergetic model CO100 is preferable to the ordinary model CO60. The apparent discrepancy that still exists between the CO100 and observations might be related to the morphology of the ejecta, i.e., its deviation from spherical symmetry, as was also suggested in the case of SN 1998bw (Höflich, Wheeler, & Wang 1998; Iwamoto et al. 1998). This issue will be discussed in § 5.1.

4. SYNTHETIC SPECTRA

To strengthen the arguments in § 3.3, we compare the observed spectra with theoretical model spectra computed using our explosion models with a more sophisticated spectrum synthesis code (Mazzali & Lucy 1993; Lucy 1999; Mazzali 1999). With such a detailed spectrum synthesis, we can distinguish between different models more clearly because the spectrum contains much more information than a single-band light curve.

Around maximum light, the spectra of SN 1997ef show just a few very broad features and are quite different from those of ordinary SNe Ib/c but similar to those of SN 1998bw. However, at later epochs the spectra develop features that are easy to identify, such as the Ca II IR triplet at ~ 8200 Å, the O I absorption at 7500 Å, several Fe II features in the blue, and they look very similar to the spectrum of the ordinary SN Ic SN 1994I.

We computed synthetic spectra with a Monte Carlo spectrum synthesis code using the density structure and composition of the hydrodynamic models CO60 and CO100. The code is based on the pure scattering code described by Mazzali & Lucy (1993) but has been improved to include photon branching, so that the reprocessing of the radiation from the blue to the red is followed more accurately and efficiently (Lucy 1999; Mazzali 1999).

We produced synthetic spectra for three epochs near maximum of SN 1997ef: November 29, December 5, and December 17. These are early enough that the spectra are

TABLE 3

PARAMETERS OF THE SYNTHETIC SPECTRA

Date (1997)	Epoch (days)	L (ergs s^{-1})	$v_{\rm ph}$ (km s^{-1})	$v_{\rm SiII}$ ($R_\odot$)	log $\rho_{\rm ph}$ (g cm^{-3})	Mass ($M_\odot$)	$T_{\rm eff}$ (K)	$T_{\rm bb}$ (K)	$B_{\rm mod}$	$V_{\rm mod}$	$V_{\rm obs}$	BC	$M_{\rm mod}$
Nov 29……	9	42.17	15500	19072	−12.65	0.71	6123	7666	17.45	16.75	16.7	0.28	−16.700
Dec 5 …….	15	42.19	9500	13962	−12.30	3.02	6128	9407	17.35	16.63	16.5	0.35	−16.750
Dec 17 ……	27	42.24	7500	8011	−12.67	4.79	5291	6697	17.70	16.59	16.6	0.26	−16.875

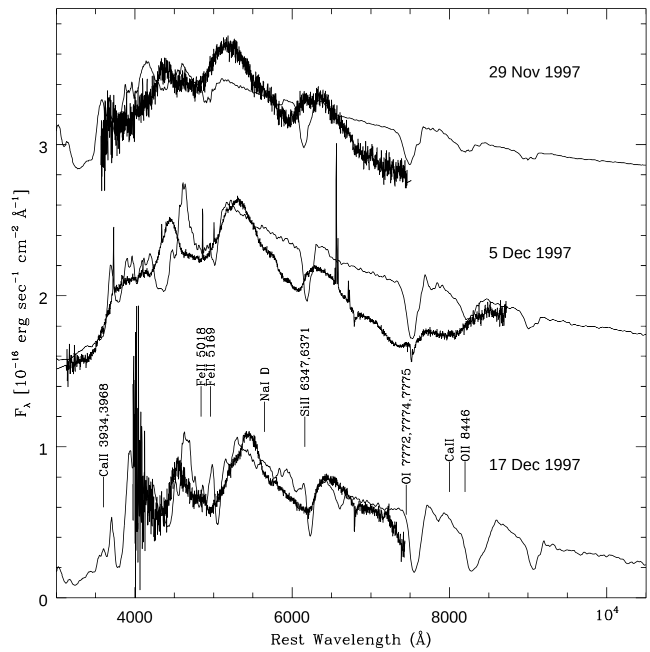

FIG. 8.—Observed spectra of SN 1997ef (*bold lines*) and synthetic spectra computed using model CO60. The line features seen in the synthetic spectra are much too narrow compared with observations.

very sensitive to changes in the kinetic energy. As in the light-curve comparison, we adopted a distance modulus of $\mu = 33.6$ mag, and $E(B-V) = 0.00$. The model parameters, the computed temperatures, and the magnitudes of the synthetic spectra for CO100 are listed in Table 3.

In Figure 8 we show the synthetic spectra computed with the ordinary SN Ic model CO60. The lines in the spectra computed with this model are always much narrower than the observations. This clearly indicates a lack of material at high velocity in model CO60 and suggests that the kinetic energy of this model is much too small.

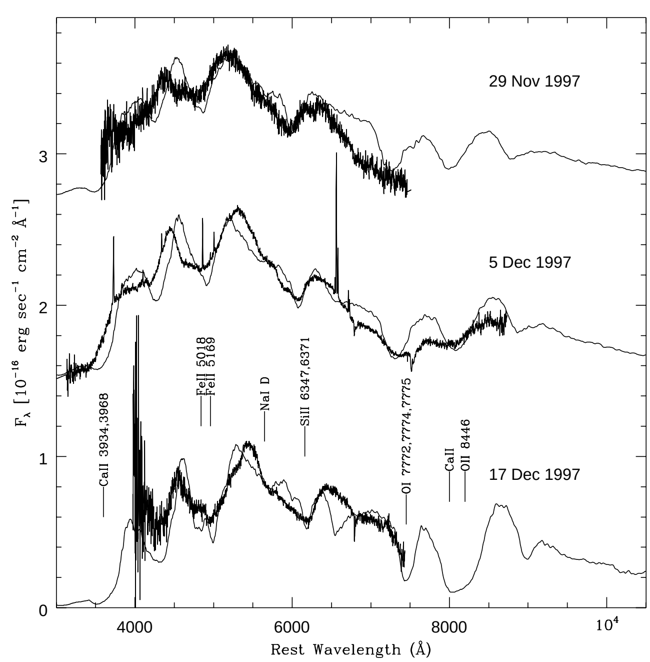

FIG. 9.—Comparison between the observed spectra of SN 1997ef (*bold lines*) and synthetic spectra computed using model CO100 (*solid lines*). The fits are much improved with CO100 compared with the ones with CO60.

Synthetic spectra obtained with the hypernova model CO100 for the same three epochs are shown in Figure 9. The spectra show much broader lines and are in good agreement with the observations. In particular, the blending of the Fe lines in the blue, giving rise to broad absorption troughs, is well reproduced, and so is the very broad Ca-O feature in the red. The two "emission peaks" observed at $\sim$4400 and 5200 Å correspond to the only two regions in the blue that are relatively line-free. A similar situation is observed in SN 1998bw (Iwamoto et al. 1998).

The spectra are characterized by a low temperature, even near maximum, because the rapid expansion combined with the relatively low luminosity (from the tail of the light curve, we deduce that SN 1997ef produced about 0.15 $M_\odot$ of ^{56}Ni, compared to about 0.6 $M_\odot$ in a typical SN Ia and 0.7 $M_\odot$ in SN 1998bw) leads to rapid cooling. Thus the Si II 6355 Å line is not very strong.

Although model CO100 yields rather good synthetic spectra, it still fails to reproduce the observed large width of the O I–Ca II feature in the only near-maximum spectrum that extends sufficiently far to the red (1997 December 5). An improvement can be obtained by introducing an arbitrary flattening of the density profile at the highest velocities.

Full details of the spectrum synthesis calculations, including insights on the density structure and the abundance in the ejecta will be given in a separate paper (P. A. Mazzali et al. 2000, in preparation).

5. DISCUSSION

5.1. *Possible Aspherical Effects*

We have shown that the light curve, the photospheric velocities, and the spectra of SN 1997ef are better reproduced with the hyperenergetic model CO100 than with the ordinary SN Ic model CO60. However, there remain several features that are still difficult to explain with model CO100.

1. The observed velocity of Si II decreases much more rapidly than models predict. It is as high as $\sim$30,000 km s^{-1} at the earliest phase, but it gets as low as $\sim$3000 km s^{-1} around day 50 (Fig. 7). We find that it is difficult to get such a rapid drop of the photospheric velocity not only in models CO100 and CO60 but also in other models that can reproduce the light-curve shape reasonably well. Models with higher energies and/or smaller masses would be able to reproduce the fast evolution of the photospheric velocity, but such models would inevitably produce light curves with a narrower peak and a faster tail.

2. Obviously, the observed light curve declines slower than model CO100 in the tail part, and it is also a bit flatter than the model near the maximum part (Fig. 6). Models with lower energies and/or larger masses are able to give improved fits to both the peak and the tail of the light curve. But then it gets very difficult to reproduce the large photospheric velocities observed at early times in SN 1997ef.

This dilemma might be overcome if we introduce multiple components of the light curve from different parts of ejecta moving at different velocities. In fact, the discrepancies may be interpreted as a possible sign of asphericity in the ejecta: A part of ejecta moves faster than average to form the lines at such high velocities at early phases, while the other part of ejecta expands with a lower velocity so that the low-velocity Si II line comes up at later epochs. Having a low-velocity component would also make it easier to reproduce the slow tail.

3. Extensive mixing of ^{56}Ni is required to reproduce the short rise time of the light curve. According to hydrodynamical simulations of the Rayleigh-Taylor instability in the ejecta of envelope-stripped supernovae (Hachisu et al. 1991; Iwamoto et al. 1997), large-scale mixing cannot be expected to occur in massive progenitors because in the core of such massive stars, the density gradient is not steep enough around the composition interfaces. One possibility to induce such mixing in the velocity space is an asymmetric explosion (e.g., Nagataki, Shimizu, & Sato 1998). Higher velocity ^{56}Ni could reach the ejecta surface so that the effect of radioactive heating comes up as early as is required from light-curve modeling.

In order to realize higher densities at low-velocity regions without increasing the mass of ejecta significantly, it may be necessary that the explosion is somewhat aspherical. If the explosion is aspherical, the shock would be stronger and the material would expand at a larger velocity in a certain direction, while in its perpendicular direction, on the other hand, the shock would be weaker, ejecting lower velocity material. The density of the central region could be high enough for γ-rays to be trapped even at advanced phases, thus giving rise to a slowly declining tail (see Nakamura et al. 1999a for a discussion of SN 1998bw). In the extremely asymmetric cases, the material ejection may happen in a jetlike form. A jet could easily bring some ^{56}Ni from the deepest layer to the surface of high velocity. Detailed spectral analysis of observed spectra for different epochs are necessary to investigate this issue further.

5.2. *Gamma-Ray Bursts/Supernovae Connection and SN 1997ef*

There have been an increasing number of candidates for the gamma-ray burst (GRB)/supernova connection, including GRB 980425/SN 1998bw (Galama et al. 1998; Iwamoto et al. 1998; Iwamoto 1999), GRB 970514/SN 1997cy (Germany et al. 2000; Turatto et al. 2000), GRB 980910/SN 1999E (Thorsett & Hogg 1999). Two other high-z GRBs may also be associated with supernovae: GRB 980326 (Bloom et al. 1999) and GRB 970228 (Reichart 1999; Galama et al. 2000). The optical transients of these GRBs showed significant reddening and temporal slow-down (even with a second maximum) in their late light curves, which can be fitted by the early power-law decay plus the redshifted light curve of SN 1998bw.

As noted in § 1, a possible connection between SN 1997ef and GRB 971115 has been suggested (Wang & Wheeler 1998). Recently another SN Ic, SN 1998ey, showed a spectrum with very broad features, very similar spectra to those of SN1997ef on December 17 (Garnavich, Jha, & Kirshner 1998), but no GRB counterpart has been proposed for SN 1998ey. Although this may cast some doubt on the general association between hypernovae and GRBs, it must be noted that both SNe 1997ef and 1998ey were less energetic events than SN 1998bw. It is possible that a weaker explosion is less efficient in collimating the γ-rays to give rise to a detectable GRB (GRB 980425 was already quite weak in gamma-rays compared to the average GRBs) or that some degree of inclination of the beam axis to the line-of-sight results in a seemingly weaker supernova and in the nondetection of a GRB. Only the accumulation of more data will allow us to address these questions.

5.3. *The Mass of Ejected* ^{56}Ni

For the study of the chemical evolution of galaxies, it is important to know the mass of ^{56}Ni, $M(^{56}\mathrm{Ni})$, synthesized in core-collapse supernovae as a function of the main-sequence mass M_{ms} of the progenitor star (e.g., Nakamura et al. 1999b). From our analysis of SN 1997ef, we can add a new point on this diagram.

We evaluate the uncertainty in our estimates of $M(^{56}\mathrm{Ni})$ and M_{ms}. We need 0.15 $M_{\odot}$ of ^{56}Ni to get a reasonable fit to the light curve of SN 1997ef at a distance $D = 52.3$ Mpc. The expected 10% uncertainty in the distance leads to a 20% uncertainty in the ^{56}Ni mass, i.e., $M(^{56}\mathrm{Ni}) = 0.15 \pm 0.03\ M_{\odot}$. The distribution of ^{56}Ni affects the peak luminosity somewhat, but the effect is found to be much smaller than that of the uncertainty in the distance. A 10 $M_{\odot}$ C+O star corresponds to a $M_{\mathrm{ms}} = 30$–$35\ M_{\odot}$, but the uncertainty involved in the conversion of the core mass to M_{ms} may involve a larger uncertainty if the progenitor undergoes a close binary evolution.

Figure 10 shows $M(^{56}\mathrm{Ni})$ against M_{ms} obtained from fitting the optical light curves of SNe 1987A, 1993J, and 1994I (e.g., Shigeyama & Nomoto 1990; Nomoto et al. 1993, 1994; Shigeyama et al. 1994; Iwamoto et al. 1994; Woosley et al. 1994; Young, Baron, & Branch 1995). The amount of ^{56}Ni appears to increase with increasing M_{ms} of the progenitor, except for SN II SN 1997D (Turatto et al. 1998).

This trend might be explained as follows. Stars with $M_{\mathrm{ms}} \lesssim 25\ M_{\odot}$ form a neutron star, producing $\sim 0.08 \pm 0.03\ M_{\odot}$ ^{56}Ni as in SN IIb SN 1993J, SN Ic SN 1994I, and SN 1987A (although SN 1987A may be a borderline case between neutron star and black hole formation). Stars with $M_{\mathrm{ms}} \gtrsim 25\ M_{\odot}$ form a black hole (e.g., Ergma & van den Heuvel 1998); whether they become hypernovae or ordinary SNe II may depend on the angular momentum in the collapsing core. For SN 1997D, because of the large gravitational potential, the explosion energy is so small that most of ^{56}Ni fell back onto a compact star remnant; the fallback might cause the collapse of the neutron star into a black hole. The core of SN II SN 1997D might not have a large angular momentum because the progenitor had a massive H-rich envelope so that the angular momentum of the core might have been transported to the envelope possibly via a magnetic field effect. Similarly, a negligible amount of ejection of ^{56}Ni in black hole formation has recently been suggested for X-ray Nova Sco (GRO

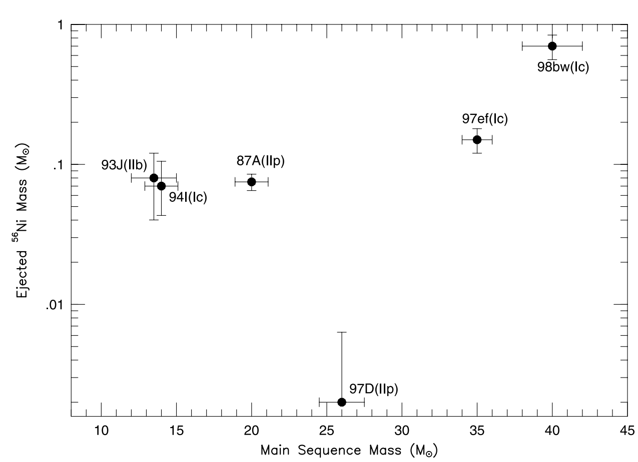

FIG. 10.—Ejected ^{56}Ni mass vs. the main-sequence mass of the progenitors of several bright supernovae obtained from light-curve models.

J1655−40), where the companion star of the black hole seems to be enriched with S, Si, Mg, and O but not Fe (Israelian et al. 1999). Hypernovae such as SNe 1998bw, 1997ef, and 1997cy might have rapidly rotating cores owing possibly to the spiraling-in of a companion star in a binary system. The outcome certainly depends also on mass-loss rate and binarity.

As noted in § 5.2, it has been claimed that the optical afterglows of GRB's 980326 and 970228 are better reproduced if a redshifted light curve of SN 1998bw is superposed on the power-law light component (Bloom et al. 1999; Reichart 1999; Galama et al. 2000). A question arising from these two examples is whether the supernovae associated with GRBs have a uniform maximum luminosity, i.e., whether 0.7 $M_{\odot}$ ^{56}Ni production as in SN 1998bw is rather common or not. However, the present study of SN 1997ef shows that the ^{56}Ni mass and thus intrinsic maximum brightness of SN 1997ef is smaller than in SN 1998bw by a factor of 4–5 (see the next subsection). We certainly need more examples for defining the luminosity function and the actual distribution of masses of ^{56}Ni produced in supernovae/hypernovae.

5.4. *Possible Evolutionary Scenarios*

Here we classify possible evolutionary paths leading to C+O star progenitors. In particular, we explore the paths to the progenitors that have rapidly rotating cores with a special emphasis because the explosion energy of hypernovae may be extracted from rapidly rotating black holes (Blandford & Znajek 1977).

1. Case of a single star: If the star is as massive as $M_{\rm ms} \gtrsim 40\ M_{\odot}$, it could lose H and He envelopes in a strong stellar wind (e.g., Schaller et al. 1992). This would be a Wolf-Rayet star.

2. Case of a close binary system: Suppose we have a close binary system with a large mass ratio. In this case, the mass transfer from star 1 to star 2 inevitably takes place in a nonconservative way, and the system experiences a common envelope phase in which star 2 is spiraling into the envelope of star 1. If the spiral-in releases enough energy to remove the common envelope, we are left with a bare He star (star 1) and a main-sequence star (star 2), with a reduced separation. If the orbital energy is too small to eject the common envelope, the two stars merge to form a single star (e.g., van den Heuvel 1994).

a) For the nonmerging case, possible channels from the He stars to the C+O stars are as follows (Nomoto, Iwamoto, & Suzuki 1995).

i) Small-mass He stars tend to have large radii, so that they can fill their Roche lobes more easily and lose most of their He envelope via Roche lobe overflow.

ii) On the other hand, larger mass He stars have radii too small to fill their Roche lobes. However, such stars have large enough luminosities to drive strong winds to remove most of the He layer (e.g., Woosley, Langer, & Weaver 1995). Such a mass-losing He star would corresponds to a Wolf-Rayet star.

Thus, from the nonmerging scenario, we expect two different kinds of SNe Ic, fast and slow, depending on the mass of the progenitor. SNe Ic from smaller mass progenitors (channel i) show faster light-curve and spectral evolutions, because the ejecta become more quickly transparent to both gamma-ray and optical photons. The slow SNe Ic originate from the Wolf-Rayet progenitors (channels ii and 1). The presence of both slow and fast SNe Ib/Ic has been noted by Clocchiatti & Wheeler (1997).

b) For the merging case, the merged star has a large angular momentum, so that its collapsing core must be rotating rapidly. It would lead to the formation of a rapidly rotating black hole from which possibly a hyperenergetic jet could emerge. If the merging process is slow enough to eject H and He envelopes, the star would become a rapidly rotating C+O star. Such C+O stars are the candidates for the progenitors of Type Ic hypernovae such as SNe 1997ef and 1998bw. If a significant amount of H-rich (or He) envelope remains after merging, the rapidly rotating core would lead to a hypernova of Type IIn possibly like SN 1997cy (or Type Ib).

6. CONCLUSIONS

We have shown that the photospheric velocities and the spectra of SN 1997ef are much better reproduced by the hyperenergetic model CO100 than by the ordinary SN Ic model CO60. The model parameters determined for CO100 are $E_K = 8 \times 10^{51}$ ergs, $M_{\rm CO} = 10\ M_{\odot}$ (which corresponds to the C+O core of a 30–35 $M_{\odot}$ star), and $M(^{56}{\rm Ni}) = 0.15\ M_{\odot}$. The compact star remnant of CO100 is as massive as $M_{\rm rem} \sim 2.4\ M_{\odot}$, thus possibly being a black hole. This high explosion energy would be extracted from the rapidly rotating black hole.

For SN 1997ef, $M_{\rm CO}$, $M(^{56}{\rm Ni})$, and E_K are all slightly smaller than for SN 1998bw, but SN 1997ef can certainly be regarded as a *hypernova* in terms of the kinetic energy of explosion. Therefore, we suggest that SNe 1997ef, 1998ey, and 1998bw form a new class of hyperenergetic Type Ic supernovae, which we call hypernovae. They are distinguished by their large kinetic energies, 8–60 times larger than in ordinary supernovae.

The smaller line velocities at advanced phases and the flatter light curve tail of SN 1997ef than the models predict may suggest the presence of a low-velocity, relatively dense core, while its higher line velocities at early phases imply the presence of a component of ejecta with yet higher velocity. These are very difficult to be reconciled with any spherically symmetric models, even with the high-energy spherical model CO100. This discrepancy between models and the observations, as well as the extensive mixing of ^{56}Ni required to explain the early rise of the light curve, seems to indicate that the explosion of SN 1997ef was at least somewhat aspherical.

This work was started at the Institute for Theoretical Physics, University of California, Santa Barbara, supported under NSF grant PHY 74-07194. We would like to thank Hideyuki Umeda, David Branch, and Nobert Langer for informative and stimulating discussion. We would also like to thank the anonymous referee for his or her useful comments and suggestions, which helped us improve the contents of the paper. This work has been supported in part by the grant-in-Aid for Scientific Research (05242102, 06233101) and COE research (07CE2002) of the Ministry of Education, Science, and Culture in Japan, and the fellowship of the Japan Society for the Promotion of Science for Japanese Junior Scientists (6728). Part of the computation was carried out on Fujitsu VPP-500 at the Institute of Physical and Chemical Research (RIKEN) and at the Institute of Space and Astronautical Science (ISAS).

REFERENCES

Arnett, W. D. 1996, Supernovae and Nucleosynthesis (Princeton: Princeton Univ. Press)
Baron, E., Hauschildt, P. H., Nugent, P., & Branch, D. 1996, MNRAS, 283, 297
Baron, E., Young, T. R., & Branch, D. 1993, ApJ, 409, 417
Blandford, R. D., & Znajek, R. L. 1977, MNRAS, 179, 433
Blinnikov, S. I. 1996, Astrophys. Lett., 22, 79
Bloom, J. S., et al. 1999, Nature, 401, 453
Clocchiatti, A., & Wheeler, J. C. 1997, ApJ, 491, 375
Colella, P., & Woodward, P. R. 1984, J. Comput. Phys., 54, 174
Eastman, R. G., & Pinto, P. A. 1993, ApJ, 412, 731
Ergma, E., & van den Heuvel, E. P. J. 1998, A&A, 331, L29
Filippenko, A. V. 1997, IAU Circ. 6783
Galama, T. J., et al. 1998, Nature, 395, 670
———. 2000, ApJ, in press
Garnavich, P., Jha, S., & Kirshner, R. 1998, IAU Circ. 7066
Garnavich, P., Jha, S., Kirshner, R., & Challis, P. 1997a, IAU Circ. 6778
———. 1997b, IAU Circ. 6798
Garnavich, P., Jha, S., Kirshner, R., Challis, P., & Balam, D. 1997c, IAU Circ. 6786
Germany, L. M., Reiss, D. L., Sadler, E. M., Schmidt, B. P., & Stubbs, C. W. 2000, ApJ, 533, 320
Hachisu, I., Matsuda, T., Nomoto, K., & Shigeyama, T. 1991, ApJ, 368, L27
Hashimoto, M. 1995, Prog. Theor. Phys., 94, 663
Hauschildt, P. H. 1992, J. Quant. Spectrosc. Radiat. Transfer, 47, 433
Hix, W. R., & Thielemann, F.-K. 1996, ApJ, 460, 869
Höflich, P., Wheeler, J. C., & Wang, L. 1999, ApJ, 521, 179
Hu, J. Y., Qiu, Y. L., Qiao, Q. Y., & Wei, J. Y. 1997, IAU Circ. 6783
Israelian, G., Rebolo, R., Basri, G., Casares, J., & Martin, E. L. 1999, Nature, 401, 142
Iwamoto, K. 1997, Ph.D. thesis, Univ. Tokyo
———. 1999, ApJ, 512, L47
Iwamoto, K., et al. 1998, Nature, 395, 672
Iwamoto, K., Nomoto, K., Höflich, P., Yamaoka, H., Kumagai, S., & Shigeyama, T. 1994, ApJ, 437, L115
Iwamoto, K., Young, T. R., Nakasato, N., Shigeyama, T., Nomoto, K., Hachisu, I., & Saio, H. 1997, ApJ, 477, 865
Karp, A. H., Lasher, G., & Chan, K. L. 1977, ApJ, 214, 161
Kurucz, R. L. 1991, in Stellar Atmospheres: Beyond Classical Models, ed. L. Crivellari, I. Hubeny, & D. G. Hummer (Dordrecht: Kluwer), 441
Lucy, L. B. 1999, A&A, 345, 211
Mazzali, A. P. 2000, A&A, in press
Mazzali, A. P., & Lucy, L. B. 1993, A&A, 279, 447
Mazzali, A. P., et al. 2000, in preparation
Mihalas, D., & Mihalas, B. W. 1984, Foundation of Radiation Hydrodynamics (Oxford: Oxford Univ. Press)
Müller, E. 1986, A&A, 162, 103
Nagataki, S., Shimizu, T. M., & Sato, K. 1998, ApJ, 495, 413
Nakamura, T., Mazzali, P.A., Nomoto, K., Iwamoto, K., & Umeda, H. 1999a, Astron. Nachr., in press
Nakamura, T., Umeda, H., Nomoto, K., Thielemann, F.-K., & Burrows, A. 1999b, ApJ, 517, 193
Nomoto, K., & Hashimoto, M. 1988, Phys. Rep., 163, 13
Nomoto, K., Iwamoto, K., & Suzuki, T. 1995, Phys. Rep., 256, 173
Nomoto, K., Suzuki, T., Shigeyama, T., Kumagai, S., Yamaoka, H., & Saio, H. 1993, Nature, 364, 507
Nomoto, K., Yamaoka, H., Pols, O. R., van den Heuvel, E. P. J., Iwamoto, K., Kumagai, S., & Shigeyama, T. 1994, Nature, 371, 227
Reichart, D. E. 1999, ApJ, 521, L111
Richmond, M. W., et al. 1996a, AJ, 111, 327
Richmond, M. W., Treffers, R. R., Filippenko, A. V., & Paik, Y. 1996b, AJ, 112, 732
Sano, S. 1997, IAU Circ. 6778
Schaller, G., Schaerer, D., Meynet, G., & Maeder, A. 1992, A&AS, 96, 269
Shigeyama, T., & Nomoto, K. 1990, ApJ, 360, 242
Shigeyama, T., Suzuki, T., Kumagai, S., Nomoto, K., Saio, H., & Yamaoka, H. 1994, ApJ, 420, 341
Swartz, D. A., & Wheeler, J. C. 1991, ApJ, 379, L13
Thorsett, S. E., & Hogg, D. W. 1999, GCN Circ. 197 (http://gcn.gsfc.nasa.gov/gcn/gcn3/197.gcn3)
Turatto, M., et al. 1998, ApJ, 498, L129
———. 2000, ApJL, in press
van den Heuvel, E. P. J. 1994, in Interacting Binaries, ed. H. Nussbaumer & A. Orr (Berlin: Springer), 263
Verner, D. A., & Yakovlev, D. G. 1995, A&AS, 109, 125
Wang, L., & Wheeler, J. C. 1998, ApJ, 504, L87
Woosley, S. E., Eastman, R. G., & Schmidt, B. P. 1999, ApJ, 516, 788
Woosley, S. E., Eastman, R. G., Weaver, T. A., & Pinto, P. A. 1994, ApJ, 429, 300
Woosley, S. E., Langer, N., & Weaver, T. A. 1995, ApJ, 448, 315
Young, T., Baron, E., & Branch, D. 1995, ApJ, 449, L51